
BAYESNMF: FAST BAYESIAN POISSON NMF WITH AUTOMATICALLY LEARNED RANK APPLIED TO MUTATIONAL SIGNATURES

A PREPRINT

 **Jenna M. Landy**

Harvard University

jlandy@g.harvard.edu

Nishanth Basava

McCallie School

nishanth.basava123@gmail.com

 **Giovanni Parmigiani**

Dana Farber Cancer Institute

Harvard University

gp@jimmy.harvard.edu

February 27, 2025

ABSTRACT

Bayesian Non-Negative Matrix Factorization (NMF) is a method of interest across fields including genomics, neuroscience, and audio and image processing. Bayesian Poisson NMF is of particular importance for counts data, for example in cancer mutational signatures analysis. However, MCMC methods for Bayesian Poisson NMF require a computationally intensive augmentation. Further, identifying latent rank is necessary, but commonly used heuristic approaches are slow and potentially subjective, and methods that learn rank automatically are unable to provide posterior uncertainties. In this paper, we introduce `bayesNMF`, a computationally efficient Gibbs sampler for Bayesian Poisson NMF. The desired Poisson-likelihood NMF is paired with a Normal-likelihood NMF used for high overlap proposal distributions in approximate Metropolis steps, avoiding augmentation. We additionally define Bayesian factor inclusion (BFI) and sparse Bayesian factor inclusion (SBFI) as methods to identify rank automatically while preserving posterior uncertainty quantification on the learned matrices. We provide an open-source R software package with all models and plotting capabilities demonstrated in this paper on GitHub at [jennalandy/bayesNMF](https://github.com/jennalandy/bayesNMF). While our applications focus on mutational signatures, our software and results can be extended to any use of Bayesian Poisson NMF.

Keywords Non-negative matrix factorization · Efficient Bayesian computation · Gibbs sampling · Mutational signatures analysis · Poisson augmentation

1 Introduction

Non-Negative Matrix Factorization (NMF) is a widely used unsupervised technique for dimension reduction and intuitive parts-based representation [Lee and Seung, 1999]. In cancer genomics, Poisson NMF is applied to mutational counts to model cancer mutational processes with latent factors called mutational signatures, assuming multiple processes contribute additively to tumor genomes [Alexandrov et al., 2013]. The Bayesian formulation of Poisson NMF allows for uncertainty quantification and integration of prior knowledge.

The computational cost of MCMC methods (e.g., Gibbs samplers) for Bayesian NMF grows with both the number of samples and the number of latent factors considered. Using a Poisson likelihood requires Poisson augmentation, which introduces additional latent variables, and thus additional Gibbs updates, resulting in computational requirements far exceeding that of a Bayesian Normal NMF [Cemgil, 2009]. With growing publicly available data sources for mutational signatures analysis [Consortium, 2010, Weinstein et al., 2013, Consortium, 2020] and a growing reference set of previously discovered mutational signatures [Alexandrov et al., 2020], computational efficiency is a key consideration for work in this field.

Identifying the latent rank is a fundamental aspect of any factor model. Most Bayesian NMF methods take a heuristic approach: they fit a separate model for each rank considered and optimize regularized metrics such as Bayesian information criterion (BIC) [Rosales et al., 2016, Gori and Baez-Ortega, 2018] or subjectively determine the “elbow” of metrics like mean squared error (MSE) or cosine similarity [Gori and Baez-Ortega, 2018, Islam et al., 2022]. This is a computationally intensive process and requires post-hoc, and potentially subjective, model selection. Existing methods that automatically learn rank as a part of the Bayesian model with automatic relevance determination (ARD) do so by optimizing the posterior numerically, meaning they are fast but result in point estimates without posterior uncertainties [Kasar et al., 2015, Kim et al., 2016]. Another recent method, compNMF [Zito and Miller, 2024], is able to learn rank automatically while maintaining posterior uncertainty, but it does not ease the computational burden of Poisson augmentation.

In this paper, we introduce a computationally efficient Gibbs sampler for Bayesian Poisson NMF which automatically determines the number of latent factors while quantifying uncertainties of the learned matrices. We avoid the computationally intensive Poisson augmentation by pairing the desired Poisson-likelihood NMF with a Normal-likelihood NMF for high-overlap proposals in approximate Metropolis sampling. We provide an open-source R software package, bayesNMF, with all models and plotting capabilities demonstrated in this paper on GitHub at [jennalandy/bayesNMF](https://github.com/jennalandy/bayesNMF). We demonstrate the accuracy and efficiency of this approach through simulation studies and apply it to mutational counts matrices of 20 cancer types from the Pan Cancer Analysis of Whole Genomes (PCAWG) database [Consortium, 2020].

2 Background

2.1 Cancer Mutational Signatures

Cancer is caused by the accumulation of somatic mutations, which in turn are caused by various mutational processes working at once. Understanding which mutational processes are active in a tumor genome can improve our understanding of cancer development, and may answer questions about subtyping, prognosis, and treatment [Nik-Zainal et al., 2012a,b, Alexandrov et al., 2013, Rosales et al., 2016]. A computationally-derived mutational signature models the specific mutational patterns produced by a mutational process. Previously discovered signatures have been associated with known mutational pathways, including DNA damage repair deficiencies [Zámborszky et al., 2017] and the deamination of 5-methylcytosine [Nik-Zainal et al., 2012a] as well as those resulting from tobacco smoke [Alexandrov et al., 2013, Nik-Zainal et al., 2015] and ultraviolet radiation [Nik-Zainal et al., 2015, Saini et al., 2016, Hayward et al., 2017]. The Catalog of Somatic Mutations in Cancer (COSMIC) [Tate et al., 2019] database provides a high-confidence set of reference signatures that, though useful for comparison, were estimated from data so cannot be treated as ground truth.

Mutational signatures are learned through non-negative matrix factorization (NMF) or Bayesian NMF on a mutational counts matrix with K mutation types as rows and G samples, or tumor genomes, as columns. This decomposition results in a signatures matrix, P , holding relative frequencies with which each signature gives rise to each mutation type, and an exposures matrix, E , with relative contributions of each signature to each sample. Single base substitution (SBS) mutations are often categorized by the substitution and its immediate left and right contexts (e.g., A[C>T]G). Base pairing maps all center mutations to originate with Thymine (T>·) or Cytosine (C>·), resulting in 96 mutation types. The current standard Bayesian NMF model for mutational signatures analysis is a Poisson likelihood, most often with Gamma priors [Rosales et al., 2016, Grabski et al., 2023a, Zito and Miller, 2024], although others have used Dirichlet priors [Gori and Baez-Ortega, 2018, Zito and Miller, 2024], Truncate Normal (L2) priors [Kasar et al., 2015, Kim et al., 2016], or Exponential (L1) priors [Kasar et al., 2015, Kim et al., 2016].

Mutational signatures analysis is a quickly growing field along with an increasing number of publicly available databases, including COSMIC [Tate et al., 2019], mSignatureDB [Huang et al., 2018], the Pan Cancer Analysis of Whole Genomes (PCAWG) [Consortium, 2020], and the compendium of Mutational Signatures of Environmental Agents [Kucab et al., 2019]. With increased availability and sizes of data sources, computational efficiency needs to be carefully considered when making modeling and implementation choices.

2.2 Bayesian Non-Negative Matrix Factorization (NMF)

Non-negative matrix factorization (NMF) is an unsupervised method to decompose non-negative data, M , with dimension K variables by G samples, into two lower-rank non-negative matrices, P and E [Paatero and Tapper, 1994, Lee and Seung, 1999]. NMF represents each observation of the data matrix, or column of M , as a linear combination of

latent factors, or columns of P , with weights in E :

$$M_{kg} = \sum_{n=1}^N P_{kn} E_{ng}, \quad M = PE, \quad M \in \mathbb{R}_{\geq 0}^{K \times G}, P \in \mathbb{R}_{\geq 0}^{K \times N}, E \in \mathbb{R}_{\geq 0}^{N \times G}.$$

NMF uses gradient descent to minimize a reconstruction error, often the Kullback-Leibler (KL)-divergence between M and PE or the Frobenius norm of the difference $M - PE$ [Lee and Seung, 2000]. Minimizing KL-divergence is equivalent to maximizing a Poisson likelihood centered at PE [Cemgil, 2009]. Similarly, minimizing Frobenius norm is equivalent to maximizing a Normal likelihood centered at PE [Schmidt et al., 2009]:

$$\begin{aligned} \operatorname{argmin}_{P,E} KL(M||PE) &= \operatorname{argmax}_{P,E} \sum_{k,g} p_{\text{Poisson}}(M_{kg} | \lambda = (PE)_{kg}), \\ \operatorname{argmin}_{P,E} \|M - PE\|_F^2 &= \operatorname{argmax}_{P,E} \sum_{k,g} p_{\text{Normal}}(M_{kg} | \mu = (PE)_{kg}, \sigma^2). \end{aligned}$$

Once NMF is redefined probabilistically, Bayesian NMF adds priors to P and E [Cemgil, 2009, Schmidt et al., 2009]. To solve Bayesian Poisson NMF with MCMC methods, Poisson augmentation is necessary in order to separate the full conditional distributions of P and E for sampling [Cemgil, 2009]. The subset of counts from M_{kg} attributed to latent factor n , Z_{kng} , follows a Poisson distribution centered at $P_{kn} E_{ng}$ and satisfies $M_{kg} = \sum_n Z_{kng}$. This imposes $K \cdot N \cdot G$ additional Gibbs updates at each iteration, increasing the computational requirements of Bayesian Poisson NMF far beyond that of Bayesian Normal NMF.

2.3 Mutational Signatures Software

Table 1 compares bayesNMF to existing software for Bayesian NMF applied to mutational signatures analysis. To the best of our knowledge, bayesNMF is the first method to avoid Poisson augmentation and learn rank automatically while reporting posterior uncertainty.

3 bayesNMF R software package

3.1 Modeling Capabilities

The bayesNMF R software package allows users to fit all models defined in this paper with the bayesNMF function. Model specifications can be adjusted by the `likelihood` (default “poisson”) and `prior` (default “truncnormal”) parameters. The `rank` parameter can be a fixed value or a range vector. If a vector is provided, the `learn_rank_method` parameter can be set to one of the following: “heuristic” (optimizing BIC), “SBFI” (default), or “BFI”. Users are able to specify initial values (`init` parameter) as well as prior and hyperprior parameters (`prior_parameters` parameter).

The bayesNMF package implements an automated convergence detection algorithm and reports convergence metrics in a log file (Supplementary Appendix A.4). This makes it simple for beginners to use the package, reduces the subjectivity of sampler stopping, and ensures all models reach the same degree of convergence so results can be compared fairly.

3.2 Visualization Capabilities

The bayesNMF R package also provides functionality to visualize results in terms of point estimates and posterior uncertainty, and it allows comparison to a set of reference signatures if desired. The default reference is COSMIC v3.3.1 SBS signatures [Tate et al., 2019], but a custom reference matrix can also be provided to `ref_matrix` in any of these functions.

The `get_heatmap` function aligns and visualizes cosine similarities between estimated and reference signatures. The `plot_results` function allows a user to visualize one or a set of bayesNMF results objects (see Figure 3a). This figure shows which signatures are present, median mutations attributed to each signature, and the posterior mean cosine similarity between the estimated signature and its reference. This function also returns a `dataframe` storing all values used in the visualization.

Finally, the `plot_sig` function visualizes an estimated mutational signature (Figures 1e, 2e, 4a-b), displaying reference signatures as bar plots in the style of the COSMIC database [Tate et al., 2019] and maximum a-posteriori (MAP) estimates and 95% credible intervals as a point with whiskers. By default, this function will align the estimated signature to its best match in the reference, or a specific signature index or name can be passed to the `ref` parameter. This function can also be used to plot a reference or estimated signature alone.

4 Methods

4.1 Bayesian NMF with Fixed Rank

We define and implement three models for Bayesian NMF assuming the latent rank is known or fixed. Two models use standard Gibbs samplers and serve as baseline models for comparison (Table 2, white rows). We note that the first is the same Poisson-Gamma model implemented by `SigneR` [Rosales et al., 2016] and the second is the same Normal-Truncated Normal model implemented by `SignatureAnalyzer` [Kasar et al., 2015, Kim et al., 2016]. We implemented our own models to enable a more direct comparison of metrics and runtimes with everything besides likelihood and prior held constant between models (e.g., order of Gibbs updates, sampling strategies, convergence criteria, I/O operations).

The *fast* Poisson-Truncated Normal model (Table 2, grey row) uses Metropolis steps in the updates of P and E, where full conditional distributions from the Normal-Truncated Normal model are used as high-overlap proposal distributions. The proposals depend on previous values only through the chain of Gibbs updates, and we assume such dependence is approximately symmetric, making these approximate Metropolis steps. This removes the need for Poisson augmentation, reducing computational requirements to the order of the Normal model. Truncated Normal priors were chosen for

conjugacy in the proposal model. Exponential priors would also have easy-to-sample Gibbs updates, but the Truncated Normal priors are closer to Gamma priors—the current standard for mutational signatures.

Full details of model specifications, Gibbs updates, hyperparameters, convergence, inference, and reference alignment are available in Supplementary Appendices A.1-A.4.

4.2 Bayesian NMF with Learned Rank

We define three options for learning rank. The first, a heuristic approach, fits a new model for each rank considered and chooses the rank that optimizes BIC. The second and third use a Bayesian factor inclusion (BFI) approach with and without sparsity.

BFI uses a diagonal binary factor inclusion matrix, A , where $A_{nn} = 1$ if latent factor n is included in the model, and 0 if excluded, redefining the NMF problem as

$$\mathbb{E}[M_{kg}] = \sum_{n=1}^N P_{kn} A_{nn} E_{ng}, \quad \mathbb{E}[M] = PAE$$

with latent rank $N^* = \sum_{n=1}^N A_{nn}$. This is based on a strategy developed by [Grabski et al. \[2023a,b\]](#) to learn factor sharing patterns in multi-study settings.

Each factor inclusion indicator A_{nn} has a Bernoulli prior. The prior probability of factor inclusion q is determined by a random variable R , which represents the expected rank and has a uniform hyperprior between 0 and N . The value q is clipped away from 0 and 1 to avoid the Gibbs sampler getting stuck at the endpoint ranks 0 or N :

$$A_{nn} \sim \text{Bernoulli}(q),$$

$$q = \begin{cases} 0.4/N & \text{if } R = 0 \\ R/N & \text{if } R = 1, \dots, N - 1, \\ 1 - 0.4/N & \text{if } R = N \end{cases},$$

$$p(R = r) = 1/(N + 1) \text{ for } r = 0, \dots, N.$$

N is set to a large number, and the model automatically learns the posterior distribution of A , and by extension, the posterior distribution of latent rank $N^* = \sum_{n=1}^N A_{nn}$.

Including A in the model induces a highly multimodal posterior, where Gibbs samplers are likely to get caught in local modes. We adapt the tempering approach used in [Grabski et al. \[2023a\]](#) for the Gibbs updates of A and R . In tempered sampling steps, the likelihood term is raised to a temperature power γ : $A_{nn} \sim p(A_{nn})p(M|A_{nn}, \dots)^\gamma$ and $R \sim p(R)p(M|R, \dots)^\gamma$. The temperature γ progresses slowly from 0 to 1 over the course of the burn-in period. This way, early samples are from the prior alone, allowing the sampler to better explore the landscape. The likelihood gradually acquires more weight until the samples are finally from the full conditional when $\gamma = 1$.

Software Name	Lang.	Model(s) (Likelihood - Prior)	Learning Rank	Post. Uncert.	Poisson Aug.
bayesNMF	R	Poisson - Truncated Normal	BFI, SBFI, Heuristic (BIC)	Yes	No
Signature Analyzer	Python (cli)	Poisson/Normal - L1/L2	ARD	No	No
SigneR	R	Poisson - Gamma	Heuristic	Yes	Yes
SigFit	R	Multinomial/Poisson/Negative Binomial/Normal - Dirichlet	Heuristic	Yes	Yes
CompNMF	R	Poisson - Dirichlet/Gamma	Compressive	Yes	Yes

Table 1: **Existing software for Bayesian NMF applied to mutational signatures:** SignatureAnalyzer [Kasar et al., 2015, Kim et al., 2016], SigneR [Rosales et al., 2016], SigFit [Gori and Baez-Ortega, 2018], and CompNMF [Zito and Miller, 2024]. We only include software that learns signatures de-novo, excluding those that re-fit to reference signatures. For each software, we report the programming language, model(s) implemented in terms of likelihood-prior combinations, how latent rank is learned, whether posterior uncertainty is reported on the resulting factor and weight matrices, and whether computationally intensive Poisson augmentation is required. [BFI: Bayesian factor inclusion. SBFI: sparse Bayesian factor inclusion. ARD: automatic relevance determination. L1: equivalent to an Exponential prior. L2: equivalent to a Truncated Normal prior.]

Model	Likelihood	Priors	Hyperpriors	Aug.
Poisson-Gamma	$Z_{kng} \sim \text{Poisson}(P_{kn}E_{ng})$ $M_{kg} = \sum_n Z_{kng}$	$P_{kn} \sim \text{Gamma}(\alpha_{kn}^P, \beta_{kn}^P)$ $E_{ng} \sim \text{Gamma}(\alpha_{ng}^E, \beta_{ng}^E)$	$\alpha_{kn}^P \sim \text{Gamma}(c_{kn}^P, d_{kn}^P)$ $\alpha_{ng}^E \sim \text{Gamma}(c_{ng}^E, d_{ng}^E)$ $\beta_{kn}^P \sim \text{Gamma}(a_{kn}^P, b_{kn}^P)$ $\beta_{ng}^E \sim \text{Gamma}(a_{ng}^E, b_{ng}^E)$	Yes
Normal-Truncated Normal	$M_{kg} \sim \text{Normal}((PE)_{kg}, \sigma_g^2)$	$P_{kn} \sim \text{TN}_{[0, \infty)}(\mu_{kn}^P, \sigma_{kn}^{2P})$ $E_{ng} \sim \text{TN}_{[0, \infty)}(\mu_{ng}^E, \sigma_{ng}^{2E})$ $\sigma_g^2 \sim \text{IG}(\alpha_g, \beta_g)$	$\mu_{kn}^P \sim \text{Norm}(m_{kn}^P, s_{kn}^P)$ $\mu_{ng}^E \sim \text{Norm}(m_{ng}^E, s_{ng}^E)$ $\sigma_{kn}^{2P} \sim \text{IG}(a_{kn}^P, b_{kn}^P)$ $\sigma_{ng}^{2E} \sim \text{IG}(a_{ng}^E, b_{ng}^E)$	No
Fast Poisson-Truncated Normal	$M_{kg} \sim \text{Poisson}((PE)_{kg})$	$P_{kn} \sim \text{TN}_{[0, \infty)}(\mu_{kn}^P, \sigma_{kn}^{2P})$ $E_{ng} \sim \text{TN}_{[0, \infty)}(\mu_{ng}^E, \sigma_{ng}^{2E})$ $\sigma_g^2 \sim \text{IG}(\alpha_g, \beta_g)$	$\mu_{kn}^P \sim \text{Norm}(m_{kn}^P, s_{kn}^P)$ $\mu_{ng}^E \sim \text{Norm}(m_{ng}^E, s_{ng}^E)$ $\sigma_{kn}^{2P} \sim \text{IG}(a_{kn}^P, b_{kn}^P)$ $\sigma_{ng}^{2E} \sim \text{IG}(a_{ng}^E, b_{ng}^E)$	No

Table 2: bayesNMF **model specifications for fixed rank** and whether Poisson augmentation is needed. In the fast Poisson-Truncated Normal model, we define priors for and update the variables σ_g^2 for use in the proposal distributions of P and E . Full details are available in Supplementary Appendix A.1. [TN: Truncated Normal, indexed by lower and upper bounds. IG: Inverse Gamma. Aug: Poisson augmentation. Second parameter of all Normal distributions is variance.]

Sparse Bayesian factor inclusion (SBFI) replaces the likelihood in the Gibbs update of A_{nn} with $e^{-\frac{1}{2}BIC}$ to encourage sparsity in the latent rank:

$$BIC = -2 \cdot \log [p(M|A_{nn} = a, \dots)] + \log(G) \cdot (K + G)N^{(a)}$$

$$p(A_{nn} = a|\dots) \propto p(A_{nn} = a) \cdot \left[e^{-\frac{1}{2}BIC} \right]^\gamma = q^a(1 - q)^{1-a} \cdot \left[p(M|A_{nn} = a, \dots) \cdot G^{-\frac{1}{2}(K+G)N^{(a)}} \right]^\gamma$$

where $N^{(a)} = \sum_{n'} A_{n'n'}$ when $A_{nn} = a$, G is the sample size, and $(K + G)N^{(a)}$ is the number of functional parameters in the matrices P and E . Once tempering is done and $\gamma = 1$, this is equivalent to the Gibbs update as if A_{nn} had the sparse prior

$$p(A_{nn} = 1) = \frac{qG^{-\frac{1}{2}(K+G)}}{qG^{-\frac{1}{2}(K+G)} + (1 - q)}.$$

Again, full details of model specifications, Gibbs updates, hyperparameters, convergence, inference, and reference alignment are available in Supplementary Appendices A.1-A.4.

4.3 Metrics

We evaluate fixed-rank NMF solutions in terms of their ability to reconstruct the original data matrix and latent factors as well as total runtime. Reconstruction error is measured in terms of RMSE and KL-divergence between the data matrix M and estimated \hat{M} , defined as the average over posterior samples $M^{(i)} = P^{(i)}E^{(i)}$.

Factor accuracy is measured after alignment as the minimum (worst) cosine similarity between true P and estimated \hat{P} , with \hat{P} defined as the average over posterior samples $P^{(i)}$. We align signatures based on cosine similarity and assume that each estimated signature must be assigned to a unique reference signature (see Supplementary Appendix A.5).

Learned-rank NMF solutions are evaluated by their sensitivity and precision as well as the accuracy of estimated rank. Sensitivity is the proportion of true signatures for which there is an estimated signature with cosine similarity >0.9 and is penalized by underestimation of rank because there will be at least one true signature without an estimated match. Precision is the proportion of estimated signatures for which there is a true signature with cosine similarity >0.9 and is penalized by overestimation of rank when additional signatures are noise, but not if additional signatures are duplicates. Precision may also be penalized by underestimation of rank in the case that estimated signatures are combinations of true signatures, but not if one or more true signatures are simply excluded.

5 Simulation Studies

5.1 Bayesian NMF with Fixed Rank

In simulations, we consider true latent ranks $N \in [2, 4, 8, 16]$ where N signatures (that sum to 1) are randomly sampled from COSMIC SBS v3.3.1 [Tate et al., 2019], and we consider sample sizes $G \in [16, 32, 64, 128]$ for $G \geq 8 \cdot N$. We create 10 datasets for each N, G combination. The expected number of mutations in sample g is generated

$m_g \sim \text{Negative Binomial}(r \cdot N, p)$, with $r = 111.11$ and $p = 0.1$ yielding $E[m_g] = 1000 \cdot N$, or 1000 mutations per signature in each sample, on average. This ensures each simulation provides comparable relative power towards each signature. Each column of the exposures matrix, E , is generated $E_g \sim \text{Multinomial}(m_g, \mathbf{p})$, where $\mathbf{p} \sim \text{Dirichlet}(\mathbf{1}_N)$. Using multinomial priors for exposures and fixed values for signatures means that no model correctly specifies the prior distributions. Mutational counts are simulated $M_{kg} \sim \text{Poisson}(\lambda_{kg} = (PE)_{kg})$.

Figure 1a shows the minimum cosine similarity of signatures is nearly always above 0.9 and is almost identical between the models. Even though the data is Poisson-generated, the Normal and Poisson models result in similar estimated signatures—this validates our use of the Normal-Truncated Normal full conditional distributions as high-overlap proposals for the fast Poisson-Truncated Normal model. Cosine similarity decreases as the number of signatures increases.

Comparing only the two baseline models, the Normal-Truncated Normal model typically shows better RMSE, which the Normal likelihood optimizes for (Figure 1c). Similarly, the Poisson-Gamma model typically shows better KL-divergence, which the Poisson likelihood optimizes, but only for small latent ranks $N = 2, 4$. As rank increases further, the Poisson-Gamma model struggles, possibly because the large number of latent variables creates a more complex sampling distribution with more local modes (Figure 1d). Our fast Poisson-Truncated Normal model achieves the best of both baselines: it matches the Normal-Truncated Normal in RMSE while also matching the Poisson-Gamma in KL-divergence when latent rank is low, but it does not suffer in KL-divergence when rank grows.

A key result is the difference in time requirements: the Poisson-Gamma model can require hours while the Normal-Truncated Normal model stays on the order of tens of minutes (Figure 1b). The time requirement grows with sample size and latent rank for both models, but at a faster rate for the Poisson-Gamma model. As data size continues to grow, it will quickly become burdensome to fit the Poisson-Gamma model.

The fast Poisson-Truncated Normal model avoids Poisson augmentation, giving it a significant time advantage over the baseline Poisson-Gamma model (Figure 1b). It is slightly slower than the Normal-Truncated Normal model due to the added Metropolis steps, but converges without the need for additional iterations, on average (Supplementary Appendix B.1).

5.2 Bayesian NMF with Learned Rank

We move forward with the fast Poisson-Truncated Normal NMF, and from here onward we let bayesNMF refer exclusively to this model. We evaluate our three approaches to learn rank with data simulated according to Section 5.1, but with sample size $G = 64$ and true ranks N from 1 to 16. The BIC, BFI, and SBFI approaches are used to learn ranks given a range from 1 to 20. We compare these results to SignatureAnalyzer+ARD with a Poisson objective and L2 priors, which are equivalent to bayesNMF’s Truncated Normal priors.

Figure 2a shows that the bayesNMF+SBFI and bayesNMF+BIC approaches are typically able to learn ranks at and below 10, while bayesNMF+BFI and SignatureAnalyzer+ARD are prone to overestimating low ranks. Precision and sensitivity are near perfect only when low ranks are estimated correctly, showing that when rank is low, the ability

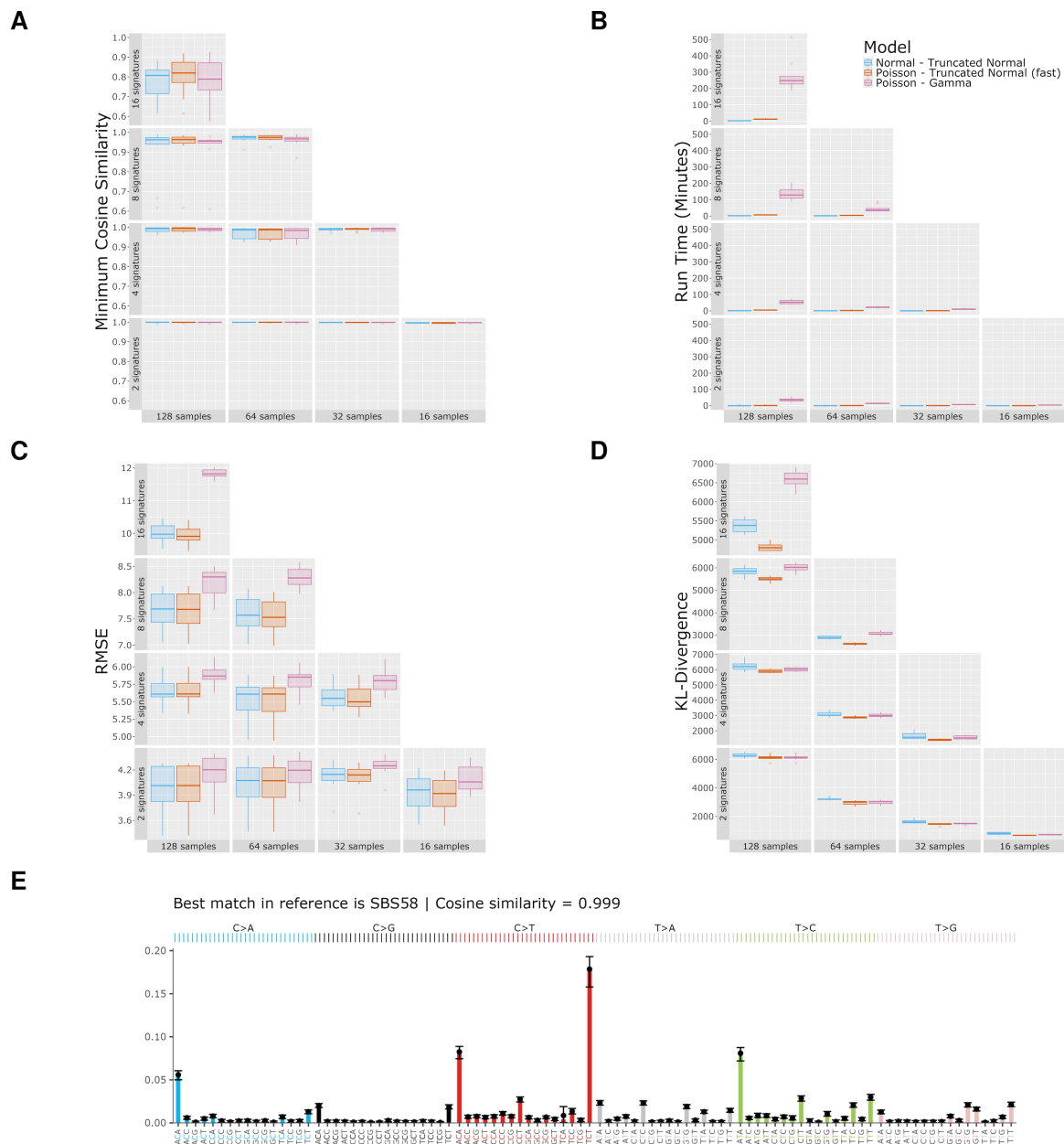


Figure 1: **Results of simulation study with known rank.** a) **Minimum cosine similarity** between estimated and true signatures. b) **Total runtime** in minutes. c) **Root mean squared error (RMSE)** between reconstructed data and true data. d) **Kullback-Leibler (KL) divergence** between reconstructed data and true data. e) **Example of a signature estimated by fast Poisson-Truncated Normal model:** bar plot for ground truth SBS58, points and whiskers for MAP estimates and 95% credible intervals (first simulation repetition of $G = 64$ samples and $N = 4$ signatures).

to reconstruct signatures depends heavily on the ability to learn rank. For ranks 10 and above, bayesNMF+BIC and SignatureAnalyzer+ARD learn rank most accurately, but precision and sensitivity show a decline in all methods. This aligns with our results from Section 5.1 that even when rank is known, signatures are not always learned correctly, especially as the number of signatures grows relative to the number of samples.

Figure 2b shows that precision is poor when rank is overestimated by bayesNMF+BFI and SignatureAnalyzer+ARD, indicating that additional signatures represent noise rather than duplicates. Precision also deteriorates for all approaches in high ranks that are underestimated, indicating that signatures are combined, not excluded, when underestimation occurs. Figure 2c shows that sensitivity is also poor with underestimation as expected.

bayesNMF+BIC outperforms bayesNMF+BFI/SBFI for higher ranks and also outperforms SignatureAnalyzer+ARD for low ranks. This comes at the cost of run time: bayesNMF+BIC averages over two hours compared to 20-30 minutes for bayesNMF+BFI/SBFI and less than three minutes for SignatureAnalyzer+ARD (Figure 2d). We emphasize, though, that the runtime of bayesNMF+BIC still benefits from the approximate Metropolis steps—the results in Section 5.1 imply that a version of bayesNMF+BIC relying on the traditional Poisson-Gamma model would take significantly longer.

6 Analysis of SBS Signatures in PCAWG Data

6.1 Data

We applied bayesNMF to the Pan-Cancer Analysis of Whole Genomes (PCAWG) [Consortium, 2020] donor-centric US-only data provided by the UCSC Xena browser [Goldman et al., 2020]. A very similar analysis was performed by Alexandrov et al. [2020] using a larger version of the PCAWG data (previously accessible on ICGC data browser <https://dcc.icgc.org/>; restricted access as of June 2024). The publicly available data includes 23 datasets, each for a different histology group or cancer type. We excluded histology groups with fewer than 10 samples, leaving 20 datasets for analysis. From the simple somatic mutation data and associated tumor histology data, we built separate mutational counts matrices for each histology group with the standard 96 mutation types.

We exclude hypermutated samples from all analyses. The inclusion of hypermutated samples during signature extraction can result in *signature bleeding*, where mutations in non-hypermutated samples are misattributed to hypermutation-specific signatures [Maura et al., 2019, Alexandrov et al., 2020]. For each histology group, we identify which samples are hypermutated by assuming the total number of mutations per sample follows a Negative Binomial mixture model, with at least a single component corresponding to non-hypermutated samples, and possibly one or more components corresponding to hypermutated samples (details in Supplementary Appendix C.1). This removes 59 samples total (<4% of data), with at most 8 samples removed per histology group in Skin-Melanoma.

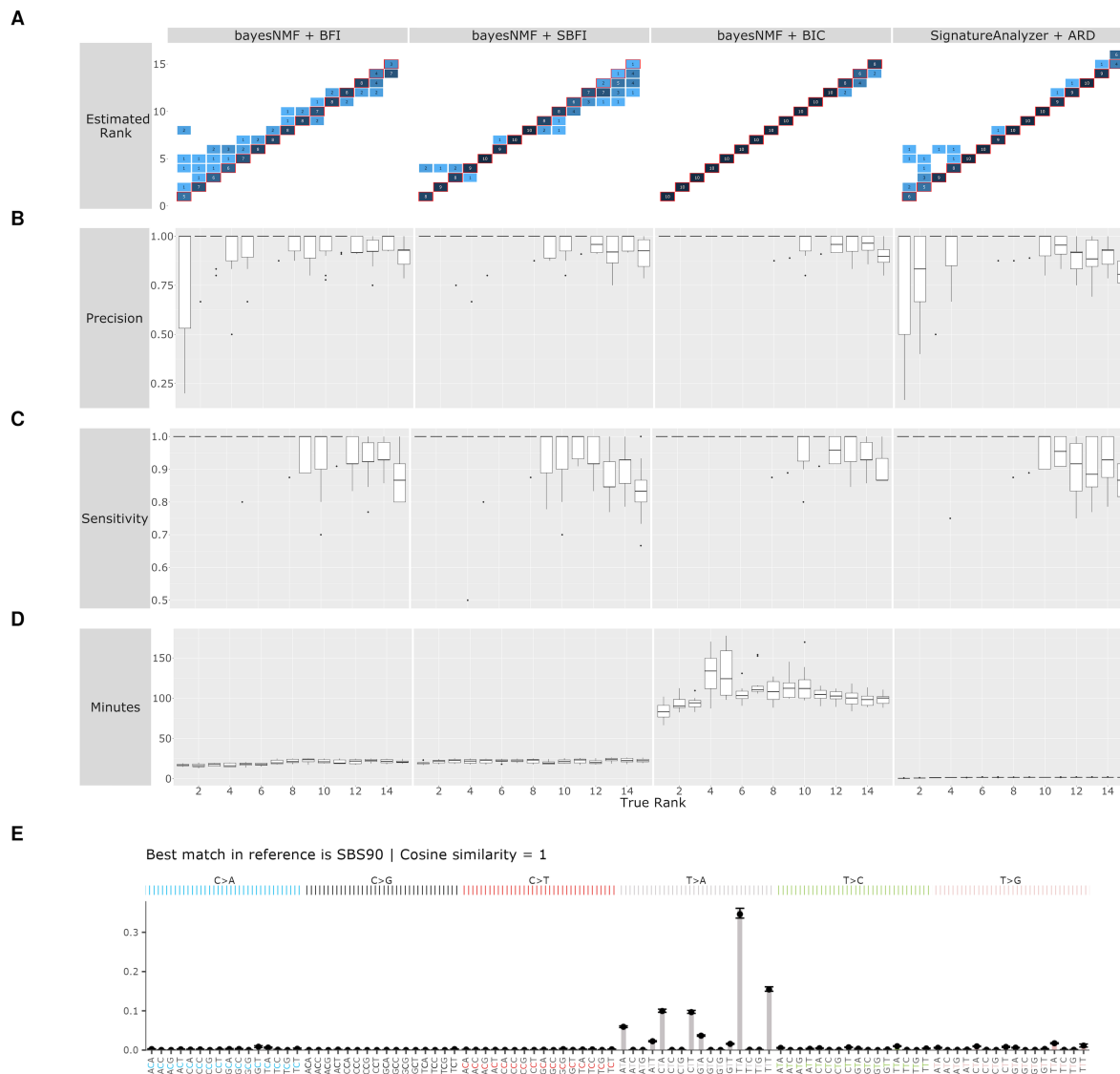


Figure 2: **Results of simulation study with unknown rank**, comparing bayesNMF with Bayesian Factor Inclusion (BFI), Sparse Bayesian Factor Inclusion (SBFI), and Heuristic (BIC), as well as SignatureAnalyzer+ARD approaches as true rank (x-axis of a-d) changes. Comparing **a) rank accuracy**: agreement between true and estimated ranks, measured as the number of occurrences, **b) precision**: proportion of estimated factors with a true factor with cosine similarity >0.9 , **c) sensitivity**: proportion of true factors with an estimated factor with cosine similarity >0.9 , and **d) total run time**. **e) Example signature estimated by bayesNMF+SBFI**: bar plot represents the ground truth SBS90, while dots and bars represent bayesNMF's MAP estimates and 95% credible intervals for each value. This signature is from the first repetition simulation of $N = 5$ signatures.

6.2 Methods

We fit bayesNMF+SBFI on each histological group separately considering ranks between 1 and 20. We use SBFI here because it balances promising metrics and computational efficiency (Section 5.2). For comparison, we also fit SignatureAnalyzer+ARD with a Poisson objective and L2 priors, which are equivalent to bayesNMF’s Truncated Normal priors. Estimated signatures are assigned to the COSMIC reference. Given the lack of ground truth in this real-world data application, we do not make claims about which method is correct or better; we simply identify the consistencies and inconsistencies between approaches.

6.3 Results

Figure 3 visualizes the results of bayesNMF+SBFI and SignatureAnalyzer+ARD aligned to the COSMIC reference signatures. These results mirror some trends from Alexandrov et al. [2020], including the presence of SBS5 and SBS40 in nearly every cancer type. All results attribute a sizeable number of mutations in B-cell non-Hodgkin lymphomas (Lymph-BNHL) to SBS9, which has a proposed etiology related to the somatic hypermutation of lymphoid cells [Alexandrov et al., 2013]. The results also all attribute a large number of mutations in esophageal adenocarcinoma (Eso-AdenoCA) to SBS17b and SBS18. Finally, all results attribute many mutations in head-and-neck tumors (Head-SCC) and ovary adenocarcinomas (Ovary-AdenoCA) to SBS13.

Our applications of both bayesNMF+SBFI and SignatureAnalyzer+ARD on this data has also revealed a notable difference from the previous work. Here, we see SBS6 as another signature present in nearly every histology group, but Alexandrov et al. [2020] learns SBS1 in its place. These signatures have a cosine similarity of 0.77, so it is possible they could be reasonably substituted for one another. The observed difference in results is likely because we utilized L2 priors while the previous work used L1 priors that encourage more “spiky” signatures. SBS1 is a spiky signature with all but four C>T mutation types near zero, while SBS5 is smoother with more non-zero values in the rest of the C>T mutations (see Supplementary Appendix C.2).

A clear difference between the bayesNMF+SBFI and SignatureAnalyzer+ARD results is the estimated rank—bayesNMF+SBFI typically results in a sparser solution, with SignatureAnalyzer+ARD frequently estimating twice the number of signatures (Figure 3d). The median estimated mutations per sample contributed by each signature is consistently above 16 in the bayesNMF+SBFI results (Figure 3a) while there are many values between 1 and 8, and some even below 1, in the SignatureAnalyzer+ARD results (Figure 3b), especially in histological groups with a large number of estimated signatures like melanoma (Skin-Melanoma) and stomach adenocarcinoma (Stomach-AdenoCA). The signatures with lower contribution counts also tend to have lower cosine similarities to the reference. This combination indicates that SignatureAnalyzer+ARD may be overfitting to noise.

Figure 3c shows which signatures are found only by one method or the other and which are found by both. We see that even when the rank estimated by bayesNMF+SBFI is lower, there are still often signatures estimated only by bayesNMF+SBFI and not by SignatureAnalyzer+ARD (e.g., SBS2 in biliary adenocarcinoma, SBS5 and 95 in

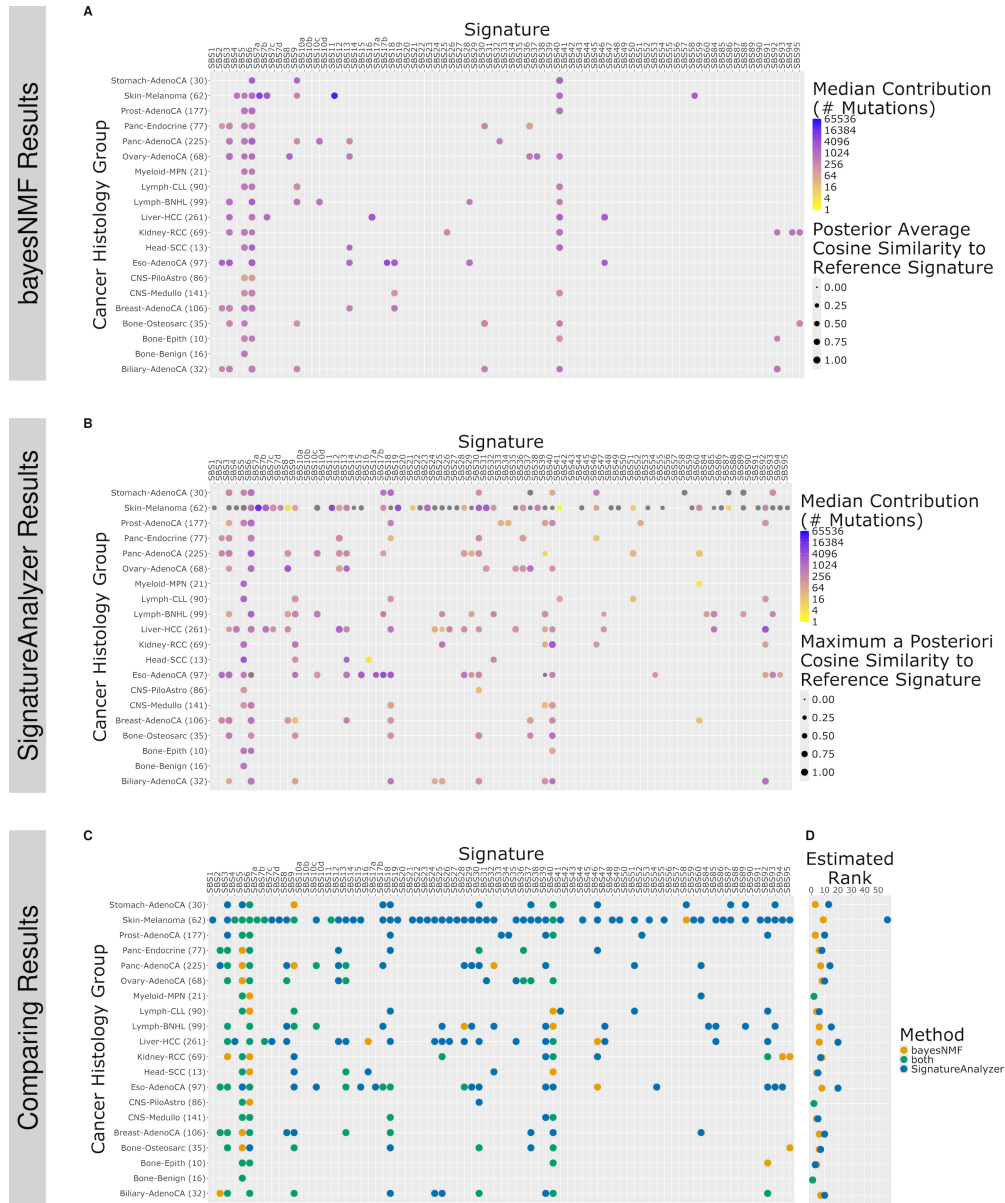


Figure 3: **Results of bayesNMF+SBFI and SignatureAnalyzer+ARD on PCAWG SBS mutations data.** **a)** Signatures identified by bayesNMF+SBFI in each histology group, sized by average posterior cosine similarity to the COSMIC reference signature and colored by median contribution among samples with nonzero mutations attributed to the signature (grey if median <1). **b)** SignatureAnalyzer+ARD results, same as a) without posterior uncertainty. **c)** Highlighting signatures identified by bayesNMF+SBFI only in orange, by SignatureAnalyzer+ARD only in blue, and by both in green. **d)** Latent ranks estimated by bayesNMF+SBFI and SignatureAnalyzer+ARD. (Figures 3a-b are inspired by Alexandrov et al. [2020] Figure 3.)

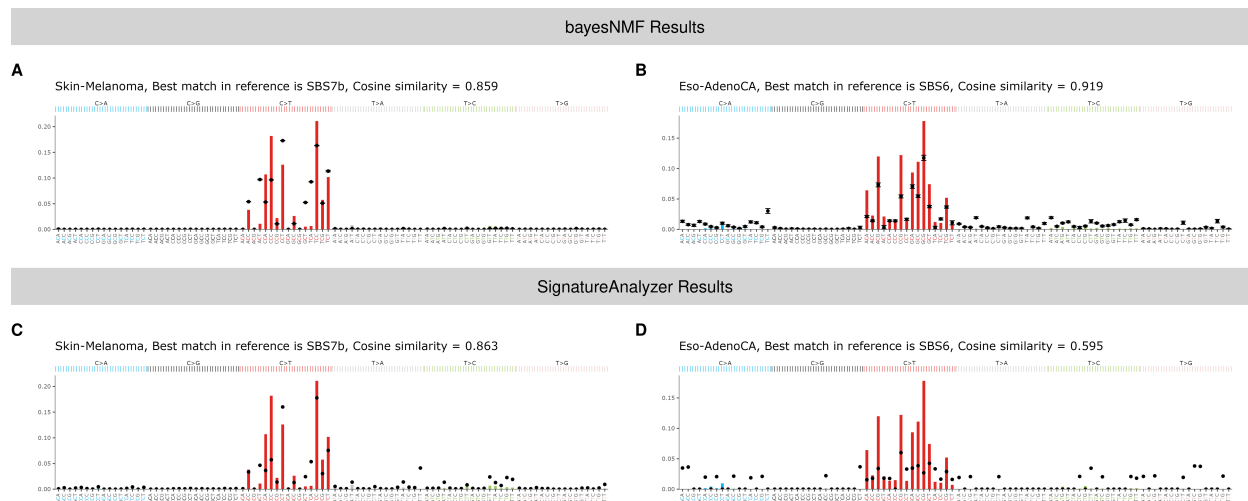


Figure 4: **Estimates of signatures SBS7b in melanoma and SBS6 in esophageal adenocarcinoma.** **a-b)** bayesNMF+SBFI estimates: bar chart for references, points for MAP estimates, error bars for 95% credible intervals. **c-d)** SignatureAnalyzer+ARD estimates, same interpretation as a-b) but without posterior uncertainty.

Bone Osteosarcoma, etc.). This means that SignatureAnalyzer+ARD isn't simply estimating additional signatures, but the two methods in fact disagree on what signatures are present.

Figure 4 compares signatures estimated by bayesNMF+SBFI and SignatureAnalyzer+ARD. The methods result in very similar estimates for SBS7b in melanoma (Skin-Melanoma), but bayesNMF+SBFI results in a higher cosine similarity to SBS6 in esophageal adenocarcinoma (Eso-AdenoCA). There are visible deviations from the COSMIC reference, and they are in the same direction for both methods even when ranks are estimated differently. This is likely due to a mismatch between the model used to learn COSMIC and the models used here. The COSMIC reference signatures were constructed using SigProfiler, where a non-Bayesian NMF extraction is followed by a sequential approach to enforce sparsity in exposures, which does not match the sparsity of bayesNMF or SignatureAnalyzer.

7 Discussion

In this paper, we introduced a computationally efficient Gibbs sampler for Bayesian Poisson NMF. This method is able to automatically determine the number of latent factors while quantifying uncertainties of the learned matrices. We provide an open-source R software package on GitHub with all models and plotting capabilities demonstrated in this paper.

The approximate Metropolis steps are the key to bayesNMF's computational efficiency. In future works, these updates could easily be used in conjunction with other approaches including multi-study NMF [Grabski et al., 2023a] or compressive NMF [Zito and Miller, 2024]. Computational efficiency will be especially important as publicly available cancer datasets grow, and we expect to see increased discussion surrounding efficient modeling and computation in the field of mutational signatures analysis.

We uncovered two examples of how the choice of model and prior can affect the learned signatures. First, the L_2 priors we used seem to preferentially learn SBS6, while L_1 priors in Alexandrov et al. [2020] learn SBS1. Second, we saw signatures estimated from PCAWG data deviate from the COSMIC reference, which may be due to a model mismatch. The impact of modeling choices on the learned signatures must be carefully considered before attributing biological meaning to mutational signatures analysis results.

We recognize a potential limitation of our assumption that each estimated signature must be assigned to a unique reference signature. It's possible that low similarity assignments could have been higher as duplicates of other signatures. However, this is a limitation only of our downstream analysis and visualization tools, not of the models themselves.

In summary, bayesNMF offers a powerful tool for exploring complex mutational landscapes, especially with its ability to report posterior uncertainty while learning rank as a part of the Bayesian model. The open-source R software package encourages usability of these methods and reproducibility of our results. As cancer genomics databases expand, bayesNMF's efficiency and flexibility make it well-suited to drive further research.

8 Acknowledgments

The authors gratefully acknowledge that this work was supported by the NIH-NIGMS training grant T32GM135117, NIH-NCI grant 5R01 CA262710-03, and NSF-DMS grant 2113707.

References

- Daniel D Lee and H Sebastian Seung. Learning the parts of objects by non-negative matrix factorization. *nature*, 401(6755):788–791, 1999.
- Ludmil B Alexandrov, Serena Nik-Zainal, David C Wedge, Samuel AJR Aparicio, Sam Behjati, Andrew V Biankin, Graham R Bignell, Niccolo Bolli, Ake Borg, Anne-Lise Børresen-Dale, et al. Signatures of mutational processes in human cancer. *nature*, 500(7463):415–421, 2013.
- Ali Taylan Cemgil. Bayesian inference for nonnegative matrix factorisation models. *Computational Intelligence and Neuroscience*, 2009:1–17, 2009. doi:[10.1155/2009/785152](https://doi.org/10.1155/2009/785152). URL <http://dx.doi.org/10.1155/2009/785152>.
- International Cancer Genome Consortium. International network of cancer genome projects. *Nature*, 464(7291):993, 2010.
- John N Weinstein, Eric A Collisson, Gordon B Mills, Kenna R Shaw, Brad A Ozenberger, Kyle Ellrott, Ilya Shmulevich, Chris Sander, and Joshua M Stuart. The cancer genome atlas pan-cancer analysis project. *Nature genetics*, 45(10):1113–1120, 2013.
- The ICGC/TCGA Pan-Cancer Analysis of Whole Genomes Consortium. Pan-cancer analysis of whole genomes. *Nature*, 578(7793):82–93, 2020.
- Ludmil B Alexandrov, Jaegil Kim, Nicholas J Haradhvala, Mi Ni Huang, Alvin Wei Tian Ng, Yang Wu, Arnoud Boot, Kyle R Covington, Dmitry A Gordenin, Erik N Bergstrom, et al. The repertoire of mutational signatures in human cancer. *Nature*, 578(7793):94–101, 2020.
- Rafael A. Rosales, Rodrigo D. Drummond, Renan Valieris, Emmanuel Dias-Neto, and Israel T. da Silva. signer: an empirical bayesian approach to mutational signature discovery. *Bioinformatics*, 33(1):8–16, 09 2016. doi:[10.1093/bioinformatics/btw572](https://doi.org/10.1093/bioinformatics/btw572). URL <http://dx.doi.org/10.1093/bioinformatics/btw572>.
- Kevin Gori and Adrian Baez-Ortega. sigfit: flexible bayesian inference of mutational signatures. *bioRxiv*, page 372896, 2018.
- SM Ashiqul Islam, Marcos Díaz-Gay, Yang Wu, Mark Barnes, Raviteja Vangara, Erik N Bergstrom, Yudou He, Mike Vella, Jingwei Wang, Jon W Teague, et al. Uncovering novel mutational signatures by de novo extraction with sigprofilerextractor. *Cell genomics*, 2(11), 2022.
- S Kasar, J Kim, R Improgo, G Tiao, P Polak, N Haradhvala, MS Lawrence, A Kiezun, SM Fernandes, S Bahl, et al. Whole-genome sequencing reveals activation-induced cytidine deaminase signatures during indolent chronic lymphocytic leukaemia evolution. *Nature communications*, 6(1):8866, 2015.
- Jaegil Kim, Kent W Mouw, Paz Polak, Lior Z Braunstein, Atanas Kamburov, Grace Tiao, David J Kwiatkowski, Jonathan E Rosenberg, Eliezer M Van Allen, Alan D D’Andrea, et al. Somatic ercc2 mutations are associated with a distinct genomic signature in urothelial tumors. *Nature genetics*, 48(6):600–606, 2016.
- Alessandro Zito and Jeffrey W Miller. Compressive bayesian non-negative matrix factorization for mutational signatures analysis. *arXiv preprint arXiv:2404.10974*, 2024.

- Serena Nik-Zainal, Ludmil B. Alexandrov, David C. Wedge, Peter Van Loo, Christopher D. Greenman, Keiran Raine, David Jones, Jonathan Hinton, John Marshall, Lucy A. Stebbings, Andrew Menzies, Sancha Martin, Kenric Leung, Lina Chen, Catherine Leroy, Manasa Ramakrishna, Richard Rance, King Wai Lau, Laura J. Mudie, Ignacio Varela, David J. McBride, Graham R. Bignell, Susanna L. Cooke, Adam Shlien, John Gamble, Ian Whitmore, Mark Maddison, Patrick S. Tarpey, Helen R. Davies, Elli Papaemmanuil, Philip J. Stephens, Stuart McLaren, Adam P. Butler, Jon W. Teague, Göran Jönsson, Judy E. Garber, Daniel Silver, Penelope Miron, Aquila Fatima, Sandrine Boyault, Anita Langerød, Andrew Tutt, John W.M. Martens, Samuel A.J.R. Aparicio, Åke Borg, Anne Vincent Salomon, Gilles Thomas, Anne-Lise Børresen-Dale, Andrea L. Richardson, Michael S. Neuberger, P. Andrew Futreal, Peter J. Campbell, and Michael R. Stratton. Mutational processes molding the genomes of 21 breast cancers. *Cell*, 149:994–1007, 2012a. doi:[10.1016/j.cell.2012.04.024](https://doi.org/10.1016/j.cell.2012.04.024).
- Serena Nik-Zainal, Peter Van Loo, David C Wedge, Ludmil B Alexandrov, Christopher D Greenman, King Wai Lau, Keiran Raine, David Jones, John Marshall, Manasa Ramakrishna, et al. The life history of 21 breast cancers. *Cell*, 149(5):994–1007, 2012b.
- Judit Zámboreszky, Bernadett Szikriszt, Judit Zsuzsanna Gervai, Orsolya Pipek, Ádám Póti, Marcin Krzystanek, Dezső Ribli, János Márk Szalai-Gindl, István Csabai, Zoltán Szallasi, et al. Loss of *brca1* or *brca2* markedly increases the rate of base substitution mutagenesis and has distinct effects on genomic deletions. *Oncogene*, 36(6):746–755, 2017.
- Serena Nik-Zainal, Jill E Kucab, Sandro Morganella, Dominik Glodzik, Ludmil B Alexandrov, Volker M Arlt, Annette Wenginger, Monica Hollstein, Michael R Stratton, and David H Phillips. The genome as a record of environmental exposure. *Mutagenesis*, 30(6):763–770, 2015.
- Natalie Saini, Steven A Roberts, Leszek J Klimczak, Kin Chan, Sara A Grimm, Shuangshuang Dai, David C Fargo, Jayne C Boyer, William K Kaufmann, Jack A Taylor, et al. The impact of environmental and endogenous damage on somatic mutation load in human skin fibroblasts. *PLoS genetics*, 12(10):e1006385, 2016.
- Nicholas K Hayward, James S Wilmott, Nicola Waddell, Peter A Johansson, Matthew A Field, Katia Nones, Ann-Marie Patch, Hojabr Kakavand, Ludmil B Alexandrov, Hazel Burke, et al. Whole-genome landscapes of major melanoma subtypes. *Nature*, 545(7653):175–180, 2017.
- John G Tate, Sally Bamford, Harry C Jubb, Zbyslaw Sondka, David M Beare, Nidhi Bindal, Harry Boutselakis, Charlotte G Cole, Celestino Creatore, Elisabeth Dawson, et al. Cosmic: the catalogue of somatic mutations in cancer. *Nucleic acids research*, 47(D1):D941–D947, 2019.
- Isabella N Grabski, Lorenzo Trippa, and Giovanni Parmigiani. Bayesian multi-study non-negative matrix factorization for mutational signatures. *bioRxiv*, pages 2023–03, 2023a. doi:[10.1101/2023.03.28.534619](https://doi.org/10.1101/2023.03.28.534619).
- Po-Jung Huang, Ling-Ya Chiu, Chi-Ching Lee, Yuan-Ming Yeh, Kuo-Yang Huang, Cheng-Hsun Chiu, and Petrus Tang. msignedb: a database for deciphering mutational signatures in human cancers. *Nucleic acids research*, 46(D1):D964–D970, 2018.

- Jill E Kucab, Xueqing Zou, Sandro Morganella, Madeleine Joel, A Scott Nanda, Eszter Nagy, Celine Gomez, Andrea Degasperi, Rebecca Harris, Stephen P Jackson, et al. A compendium of mutational signatures of environmental agents. *Cell*, 177(4):821–836, 2019.
- Pentti Paatero and Unto Tapper. Positive matrix factorization: A non-negative factor model with optimal utilization of error estimates of data values. *Environmetrics*, 5(2):111–126, 1994.
- Daniel Lee and H Sebastian Seung. Algorithms for non-negative matrix factorization. *Advances in neural information processing systems*, 13, 2000.
- Mikkel N. Schmidt, Ole Winther, and Lars Kai Hansen. *Bayesian Non-negative Matrix Factorization*, pages 540–547. Springer Berlin Heidelberg, 2009. doi:10.1007/978-3-642-00599-2_68. URL http://dx.doi.org/10.1007/978-3-642-00599-2_68.
- Isabella N Grabski, Roberta De Vito, Lorenzo Trippa, and Giovanni Parmigiani. Bayesian combinatorial multistudy factor analysis. *The annals of applied statistics*, 17(3):2212, 2023b.
- Mary J Goldman, Brian Craft, Mim Hastie, Kristupas Repečka, Fran McDade, Akhil Kamath, Ayan Banerjee, Yunhai Luo, Dave Rogers, Angela N Brooks, et al. Visualizing and interpreting cancer genomics data via the xena platform. *Nature biotechnology*, 38(6):675–678, 2020.
- Francesco Maura, Andrea Degasperi, Ferran Nadeu, Daniel Leongamornlert, Helen Davies, Luiza Moore, Romina Royo, Bachisio Ziccheddu, Xose S Puente, Herve Avet-Loiseau, et al. A practical guide for mutational signature analysis in hematological malignancies. *Nature communications*, 10(1):2969, 2019.
- Andrew Gelman, John B Carlin, Hal S Stern, and Donald B Rubin. *Bayesian data analysis*. Chapman and Hall/CRC, third edition, 1995.
- Harold W Kuhn. The hungarian method for the assignment problem. *Naval research logistics quarterly*, 2(1-2):83–97, 1955.
- Arthur P Dempster, Nan M Laird, and Donald B Rubin. Maximum likelihood from incomplete data via the em algorithm. *Journal of the royal statistical society: series B (methodological)*, 39(1):1–22, 1977.

Supplementary Material

R-package: The R-package bayesNMF is publicly available on GitHub at [jennalandy/bayesNMF](https://github.com/jennalandy/bayesNMF).

Code: All code needed to reproduce simulation studies and data analysis is publicly available on GitHub at [jennalandy/bayesNMF_PAPER](https://github.com/jennalandy/bayesNMF_PAPER).

Dataset: The PCAWG donor centric data is available on the UCSC Xena Browser at <https://xenabrowser.net/datapages/>.

A Methods Appendix

A.1 Algorithms and Gibbs Updates

For each model, we derived and implemented a Gibbs sampler. Table A.3 formally defines each model’s likelihood, priors, and hyperpriors, and provides pseudocode of the Gibbs sampler algorithms as well as the number of variables updated in each step. We note that the Poisson-Gamma model requires many more variables due to the Z_{kng} s. To put this in context, a moderately sized mutational counts matrix may have $G = 100$ samples and $K = 96$ SBS mutation types, and we may be interested in extracting at most $N = 8$ mutational signatures. The Poisson-Gamma model would have an additional $G(KN - 1) = 76,700$ parameters to update *on each iteration* compared to the Normal-Truncated Normal model.

Table A.4 lists all full conditional distributions used in the Gibbs samplers. When the latent rank is provided, the tempering parameter γ is always 1. Otherwise, γ starts at 0 and gradually reaches 1 approximately 2/5 of the way through sampling. Note that if $\gamma = 0$, the update distribution is equivalent to the prior, and if $\gamma = 1$, it is the full conditional.

A.2 Setting Hyperprior Parameters

In Bayesian regression analysis, variables are often scaled to have a convenient standard deviation to be able to set up realistic priors [Gelman et al., 1995]. However, scaling our data would not maintain counts and would not be proper for an assumed Poisson likelihood. Instead, we set hyperprior parameters to match the scale of the data such that the imposed prior distribution on the mean PE is centered at \bar{M} .

For Truncated Normal priors, we set hyperprior parameters $m_{kg}^P = m_{ng}^E = s_{kg}^P = s_{ng}^E = \sqrt{\bar{M}/N}$, $a_{kg}^P = a_{ng}^E = N + 1$, and $b_{kn}^P = b_{ng}^E = \sqrt{N}$, $\forall k, n, g$. The product of the expected mean matrices $E[\mu^P]$ and $E[\mu^E]$ has the constant \bar{M} as each element.

For Gamma priors, we set hyperprior parameters $a_{kn}^P = a_{ng}^E = 10\sqrt{N}$, $b_{kn}^P = b_{ng}^E = d_{kn}^P = d_{ng}^E = 10$, $c_{kn}^P = c_{ng}^E = 10\sqrt{\bar{M}}$. The product of expected mean matrices $E[\alpha^P]/E[\beta^P]$ and $E[\alpha^E]/E[\beta^E]$ has the constant \bar{M} as each element.

A.3 Inference

Inference is performed on the last 1000 posterior samples. When rank is fixed, maximum a-posterior (MAP) estimates of the parameters of interest, the P and E matrices, are elementwise sample averages, and 95% credible intervals are the elementwise 2.5th and 97.5th percentiles across samples.

When learning rank with BFI or SBFI, inference for P , A , and E is performed in two stages. First, we find the MAP of the discrete A matrix as its mode across the last 1000 posterior samples. Second, across the subset of samples where A matches its MAP estimate, inference on P and E is performed as it was with fixed rank.

A.4 Convergence

Common methods to check convergence of MCMC methods pose three challenges in the context of latent factor models: first, there are thousands of parameters of interest (the number of elements of the P and E matrices), which means an infeasible number of traceplots to visually inspect. Second, the scale non-identifiability of NMF (e.g., $\hat{P}\hat{E} = (2\hat{P})(\frac{1}{2}\hat{E})$) means that trace plots of values in P and E may have a slope, and thus not seem to have converged, even if the product PE is a stable solution. Third, learned latent factors may not be the same across multiple chains, so methods that compare across-chain to within-chain variation cannot be used.

We instead define a programmatic convergence criteria that is appropriate for any scale of data and ensures that the various models reach the same level of convergence. This convergence criteria is defined on a running-MAP-metrics plot, built off of the concept of a running means plot. We assume that if posterior samples have converged, then the average, or MAP, over windows of fixed lengths should not change as the window shifts, and thus a scalar metric of the MAP should not change either. In our analyses, we consider the convergence of log posterior probability with a window size of 1000 samples and window shifts of 100 samples, though the bayesNMF package also allows for convergence of BIC, log likelihood, RMSE, or KL-divergence and customization of window parameters. We determine that metrics have converged if they have improved by less than 0.1% in each of the past 10 windows considered, though this convergence criteria is customizable as well. After convergence, samples in the window with the best metric are used for final inference.

A.5 Alignment to Reference Signatures

In order to interpret and evaluate results, we frequently wish to compare estimated factors (columns of \hat{P}) to reference factors (columns of P) from previous analysis or domain knowledge, commonly from the COSMIC database [Consortium, 2020] in the case of mutational signatures. We use this approach to align estimated signatures to ground truth in our simulation studies as well.

Because matrix factorization is not scale identifiable we cannot look at scale dependent measures like MSE or KL-divergence when comparing \hat{P} to P . For this reason, we follow existing mutational signatures works [Rosales et al., 2016, Gori and Baez-Ortega, 2018, Alexandrov et al., 2020, Grabski et al., 2023a] and focus on cosine similarities between signatures.

To align estimated factors to the reference factors, we first create a similarity matrix S , where each element is the cosine similarity between a column of P and a column of \hat{P} , $S_{ij} = \cos(P_i, \hat{P}_j)$. The Hungarian algorithm [Kuhn, 1955] is used on $-1 \cdot S$, which solves the combinatorial optimization problem to reorder rows and columns to minimize the sum of values on the diagonal. The resulting aligned similarity matrix, S^* , has an optimal alignment in terms of total aligned cosine similarity. This approach only allows a single estimated signature to be aligned to each reference signature.

We incorporate posterior uncertainty into this process by performing factor alignment for each of the posterior samples used to compute \hat{P} . We determine final alignments through majority voting with cosine similarity as voting weights.

Poisson-Gamma (PG)	Normal-Truncated Normal (NT)	Fast Poisson-Truncated Normal (PT)
Model	Model	Model
<p><i>Likelihood</i></p> $Z_{kn,g} \sim \text{Poisson}(P_{kn}A_{nn}E_{ng})$ $M_{kg} = \sum_n Z_{kn,g} \sim \text{Poisson}((PAE)_{kg})$ $A_{nn} \sim \text{Depends on BFI, SBFI, or fixed rank}$	<p><i>Likelihood</i></p> $M_{kg} \sim \text{Normal}((PAE)_{kg}, \sigma_g^2)$ $A_{nn} \sim \text{Depends on BFI, SBFI, or fixed rank}$	<p><i>Likelihood</i></p> $M_{kg} \sim \text{Poisson}((PAE)_{kg})$ $A_{nn} \sim \text{Depends on BFI, SBFI, or fixed rank}$
<p><i>Priors</i></p> $P_{kn} \sim \text{Gamma}(\alpha_{kn}^P, \beta_{kn}^P)$ $E_{ng} \sim \text{Gamma}(\alpha_{ng}^E, \beta_{ng}^E)$	<p><i>Priors</i></p> $P_{kn} \sim \text{TN}(\mu_{kn}^P, \sigma_{kn}^{2P}, 0, \infty)$ $E_{ng} \sim \text{TN}(\mu_{ng}^E, \sigma_{ng}^{2E}, 0, \infty)$ $\sigma_g^2 \sim \text{InverseGamma}(\alpha_g, \beta_g)$	<p><i>Priors</i></p> $P_{kn} \sim \text{TN}(\mu_{kn}^P, \sigma_{kn}^{2P}, 0, \infty)$ $E_{ng} \sim \text{TN}(\mu_{ng}^E, \sigma_{ng}^{2E}, 0, \infty)$
<p><i>Hyperpriors</i></p> $\alpha_{kn}^P \sim \text{Gamma}(c_{kn}^P, d_{kn}^P)$ $\alpha_{ng}^E \sim \text{Gamma}(c_{ng}^E, d_{ng}^E)$ $\beta_{kn}^P \sim \text{Gamma}(a_{kn}^P, b_{kn}^P)$ $\beta_{ng}^E \sim \text{Gamma}(a_{ng}^E, b_{ng}^E)$	<p><i>Hyperpriors</i></p> $\mu_{kn}^P \sim \text{Normal}(m_{kn}^P, s_{kn}^P)$ $\mu_{ng}^E \sim \text{Normal}(m_{ng}^E, s_{ng}^E)$ $\sigma_{kn}^{2P} \sim \text{InvGamma}(a_{kn}^P, b_{kn}^P)$ $\sigma_{ng}^{2E} \sim \text{InvGamma}(a_{ng}^E, b_{ng}^E)$	<p><i>Hyperpriors</i></p> $\mu_{kn}^P \sim \text{Normal}(m_{kn}^P, s_{kn}^P)$ $\mu_{ng}^E \sim \text{Normal}(m_{ng}^E, s_{ng}^E)$ $\sigma_{kn}^{2P} \sim \text{InvGamma}(a_{kn}^P, b_{kn}^P)$ $\sigma_{ng}^{2E} \sim \text{InvGamma}(a_{ng}^E, b_{ng}^E)$
Algorithm # Steps	Algorithm # Steps	Algorithm # Steps
<p>0. Initialize $P, E, \sigma^2 \sim \text{Prior}_{PG}$</p> <p>1. Iterate:</p> <p style="padding-left: 20px;">A. $P_n \sim p_{PG}(P_n M, \dots)$ KN</p> <p style="padding-left: 20px;">B. $E_n \sim p_{PG}(E_n M, \dots)$ NG</p> <p style="padding-left: 20px;">C. $Z_{kg} \sim p_{PG}(Z_{kg} M, \dots)$ KN</p> <p style="padding-left: 20px;">D. $A_n \sim p_{PG}(A_n M, \dots)$ N</p> <p style="padding-left: 20px;">E. Update prior parameters</p> <p style="text-align: center;">$2 \cdot (KN + NG) + N$</p>	<p>0. Initialize $P, E, Z \sim \text{Prior}_{NT}$</p> <p>1. Iterate:</p> <p style="padding-left: 20px;">A. $P_n \sim p_{NT}(P_n M, \dots)$ KN</p> <p style="padding-left: 20px;">B. $E_n \sim p_{NT}(E_n M, \dots)$ NG</p> <p style="padding-left: 20px;">C. $\sigma_g^2 \sim p_{NT}(\sigma_g^2 M, \dots)$ G</p> <p style="padding-left: 20px;">D. $A_n \sim p_{NT}(A_n M, \dots)$ N</p> <p style="padding-left: 20px;">E. Update prior parameters</p> <p style="text-align: center;">$2 \cdot (KN + NG) + N$</p>	<p>0. Initialize $P, E \sim \text{Prior}_{PT}$</p> <p style="padding-left: 20px;">Initialize $\sigma^2 \sim \text{Prior}_{NT}$</p> <p>1. Iterate:</p> <p style="padding-left: 20px;">A. $P_n^* \sim p_{NT}(P_n^* M, \dots)$ KN</p> <p style="padding-left: 40px;">$\alpha = \frac{p_{PT}(P_n^* M, \dots)}{p_{PT}(P_n M, \dots)}$ N</p> <p style="padding-left: 40px;">$P_n = P_n^*$ if $u < \alpha$</p> <p style="padding-left: 40px;">for $u \sim U(0, 1)$</p> <p style="padding-left: 20px;">B. $E_n^* \sim p_{NT}(E_n^* M, \dots)$ NG</p> <p style="padding-left: 40px;">$\alpha = \frac{p_{PT}(E_n^* M, \dots)}{p_{PT}(E_n M, \dots)}$ N</p> <p style="padding-left: 40px;">$E_n = E_n^*$ if $u < \alpha$</p> <p style="padding-left: 40px;">for $u \sim U(0, 1)$</p> <p style="padding-left: 20px;">C. $\sigma_g^2 \sim p_{NT}(\sigma_g^2 M, \dots)$ G</p> <p style="padding-left: 20px;">D. $A_n \sim p_{PT}(A_n M, \dots)$ N</p> <p style="padding-left: 20px;">E. Update prior parameters</p> <p style="text-align: center;">$2 \cdot (KN + NG) + N$</p>

Table A.3: bayesNMF **model specifications and algorithms** for K features or mutation types, latent rank N , and sample size G . When rank is known or learned heuristically to optimize BIC, A is an $N \times N$ identity matrix for rank N and step D of the algorithm can be skipped. Otherwise, the prior of A depends on the method used to learn rank (see main text Section 4.2). The computational requirement of Poisson augmentation can be seen in step C of the Poisson-Gamma Algorithm. Our Fast Poisson-Truncated Normal model requires additional steps for the approximate metropolis updates, but still far fewer steps than the Poisson-Gamma. [TN: Truncated Normal, InvGamma: Inverse Gamma, PG: Poisson-Gamma, NT: Normal-Truncated Normal, PT: Fast Poisson-Truncated Normal, second parameter of Normal is always variance]

Poisson-Gamma	
Signatures P	$P_{kn} \dots \sim \text{Gamma}\left(\alpha_{kn}^P + \sum_{g=1}^G Z_{kng}, \beta_{kn}^P + \sum_{g=1}^G A_{nn}E_{ng}\right)$ $p(\alpha_{kn}^P \dots) \propto \frac{(\beta_{kn}^P)^{\alpha_{kn}^P}}{\Gamma(\alpha_{kn}^P)} P_{kn}^{(\alpha_{kn}^P-1)} (\alpha_{kn}^P)^{P_{kn}-1} e^{-d_{kn}^P \alpha_{kn}^P}$ $\beta_{kn}^P \dots \sim \text{Gamma}(a_{kn}^P + \alpha_{kn}^P, b_{kn}^P + P_{kn})$
Exposures E	$E_{ng} \dots \sim \text{Gamma}\left(\alpha_{ng}^E + \sum_{k=1}^K Z_{kng}, \beta_{ng}^E + \sum_{k=1}^K P_{kn}A_{nn}\right)$ $p(\alpha_{ng}^E \dots) \propto \frac{(\beta_{ng}^E)^{\alpha_{ng}^E}}{\Gamma(\alpha_{ng}^E)} E_{ng}^{(\alpha_{ng}^E-1)} (\alpha_{ng}^E)^{E_{ng}-1} e^{-d_{ng}^E \alpha_{ng}^E}$ $\beta_{ng}^E \dots \sim \text{Gamma}(a_{ng}^E + \alpha_{ng}^E, b_{ng}^E + E_{ng})$
Latent Variables Z	$Z_{kg} \dots \sim \text{Multinomial}\left(M_{kg}, p_n = \frac{P_{kn}E_{ng}}{\sum_n P_{kn}E_{ng}}\right)$
Signature Inclusion	$p(R=r \dots) \propto \frac{1}{N+1} \left[\prod_{n=1}^N \left(q^{(r)} \right)^{A_n} \left(1 - q^{(r)} \right)^{1-A_n} \right]^\gamma$
Indicators A	<p>where $q^{(r)} = \begin{cases} 0.4/N & \text{if } r = 0 \\ r/N & \text{if } r \in \{1, \dots, N-1\} \\ 1 - 0.4/N & \text{if } r = N \end{cases}$</p> $A_{nn} \dots \sim \text{Bernoulli}\left(\frac{p_1}{p_1+p_0}\right)$ <p>where $p_a = \begin{cases} q^a(1-q)^{1-a} \cdot f(M A_{nn}=a, \dots)^\gamma & \text{in BFI} \\ q^a(1-q)^{1-a} \cdot [f(M A_{nn}=a, \dots)] \cdot G^{-\frac{1}{2}(K+G)N^{(a)}}]^\gamma & \text{in SBFI} \end{cases}$</p> <p>and $q = q^{(R)}$</p>
Normal-Truncated Normal	
Signatures P	$P_{kn} \dots \sim \text{TN}_{[0,\infty)}\left(\mu = \frac{\mu_{kn}^P/\sigma_{kn}^{2P} + \sum_{g=1}^G A_{nn}E_{ng}(M_{kg} - \hat{M}_{kg/n})/\sigma_k^2}{1/\sigma_{kn}^{2P} + \sum_{g=1}^G A_{nn}E_{ng}^2/\sigma_k^2}, \sigma^2 = \frac{1}{1/\sigma_{kn}^{2P} + \sum_{g=1}^G A_{nn}E_{ng}^2/\sigma_k^2}\right)$ $\mu_{kn}^P \dots \sim \text{Normal}\left(\mu = \frac{m_{kn}^P/s_{kn}^E + P_{kn}/\sigma_{ng}^{2P}}{1/s_{kn}^E + 1/\sigma_{ng}^{2P}}, \sigma^2 = \frac{1}{1/s_{kn}^E + 1/\sigma_{ng}^{2P}}\right)$ $\sigma_{kn}^{2P} \dots \sim \text{InverseGamma}(a_{kn}^P + \frac{1}{2}, b_{kn}^P + \frac{1}{2}(P_{kn} - \mu_{kn}^P)^2)$
Exposures E	$E_{ng} \dots \sim \text{TN}_{[0,\infty)}\left(\mu = \frac{\mu_{ng}^E/\sigma_{ng}^{2E} + \sum_{k=1}^K P_{kn}A_{nn}(M_{kg} - \hat{M}_{kg/n})/\sigma_k^2}{1/\sigma_{ng}^{2E} + \sum_{k=1}^K P_{kn}^2 A_{nn}/\sigma_k^2}, \sigma^2 = \frac{1}{1/\sigma_{ng}^{2E} + \sum_{k=1}^K P_{kn}^2 A_{nn}/\sigma_k^2}\right)$ $\mu_{ng}^E \dots \sim \text{Normal}\left(\mu = \frac{m_{ng}^E/s_{ng}^E + E_{ng}/\sigma_{ng}^{2E}}{1/s_{ng}^E + 1/\sigma_{ng}^{2E}}, \sigma^2 = \frac{1}{1/s_{ng}^E + 1/\sigma_{ng}^{2E}}\right)$ $\sigma_{ng}^{2E} \dots \sim \text{InverseGamma}(a_{ng}^E + \frac{1}{2}, b_{ng}^E + \frac{1}{2}(E_{ng} - \mu_{ng}^E)^2)$
Variances σ^2	$\sigma_g^2 \dots \sim \text{InverseGamma}(\alpha_g + K/2, \beta_g + \frac{1}{2} \sum_k (M_{kg} - (PAE)_{kg})^2)$
Signature Inclusion	$p(R=r \dots) \propto \frac{1}{N+1} \left[\prod_{n=1}^N \left(q^{(r)} \right)^{A_n} \left(1 - q^{(r)} \right)^{1-A_n} \right]^\gamma$
Indicators A	<p>where $q^{(r)} = \begin{cases} 0.4/N & \text{if } r = 0 \\ r/N & \text{if } r \in \{1, \dots, N-1\} \\ 1 - 0.4/N & \text{if } r = N \end{cases}$</p> $A_{nn} \dots \sim \text{Bernoulli}\left(\frac{p_1}{p_1+p_0}\right)$ <p>where $p_a = \begin{cases} q^a(1-q)^{1-a} \cdot f(M A_{nn}=a, \dots)^\gamma & \text{in BFI} \\ q^a(1-q)^{1-a} \cdot [f(M A_{nn}=a, \dots)] \cdot G^{-\frac{1}{2}(K+G)N^{(a)}}]^\gamma & \text{in SBFI} \end{cases}$</p> <p>and $q = q^{(R)}$</p>

 Table A.4: **Gibbs updates** for all models.

Fast Poisson-Truncated Normal	
Signatures P	$P_{kn}^* \dots \sim \text{TN}_{[0, \infty)} \left(\mu = \frac{\mu_{kn}^P / \sigma_{kn}^{2P} + \sum_{g=1}^G A_{nn} E_{ng} (M_{kg} - \hat{M}_{kg/n}) / \sigma_k^2}{1 / \sigma_{kn}^{2P} + \sum_{g=1}^G A_{nn} E_{ng}^2 / \sigma_k^2}, \sigma^2 = \frac{1}{1 / \sigma_{kn}^{2P} + \sum_{g=1}^G A_{nn} E_{ng}^2 / \sigma_k^2} \right)$ <p>Let P^* be the current P matrix with the proposed value P_{kn}^* in place of P_{kn}</p> $acc_{kn}^P = \frac{\text{Poisson}(M P^* A E) \cdot \text{TruncNorm}(P_{kn}^* \mu_{kn}^P, \sigma_{kn}^{2P})}{\text{Poisson}(M P A E) \cdot \text{TruncNorm}(P_{kn} \mu_{kn}^P, \sigma_{kn}^{2P})}$ $P_{kn} = \begin{cases} P_{kn}^* & \text{with probability } acc_{kn}^P \\ P_{kn} & \text{with probability } 1 - acc_{kn}^P \end{cases}$ $\mu_{kn}^P \dots \sim \text{Normal} \left(\mu = \frac{m_{kn}^P / s_{kn}^E + P_{kn} / \sigma_{kn}^{2P}}{1 / s_{kn}^E + 1 / \sigma_{kn}^{2P}}, \sigma^2 = \frac{1}{1 / s_{kn}^E + 1 / \sigma_{kn}^{2P}} \right)$ $\sigma_{kn}^{2P} \dots \sim \text{InverseGamma} \left(a_{kn}^P + \frac{1}{2}, b_{kn}^P + \frac{1}{2} (P_{kn} - \mu_{kn}^P)^2 \right)$
Exposures E	$E_{ng}^* \dots \sim \text{TN}_{[0, \infty)} \left(\mu = \frac{\mu_{ng}^E / \sigma_{ng}^{2E} + \sum_{k=1}^K P_{kn} A_{nn} (M_{kg} - \hat{M}_{kg/n}) / \sigma_k^2}{1 / \sigma_{ng}^{2E} + \sum_{k=1}^K P_{kn} A_{nn} / \sigma_k^2}, \sigma^2 = \frac{1}{1 / \sigma_{ng}^{2E} + \sum_{k=1}^K P_{kn} A_{nn} / \sigma_k^2} \right)$ <p>Let E^* be the current E matrix with the proposed value E_{ng}^* in place of E_{ng}</p> $acc_{ng}^E = \frac{\text{Poisson}(M P A E^*) \cdot \text{TruncNorm}(E_{ng}^* \mu_{ng}^E, \sigma_{ng}^{2E})}{\text{Poisson}(M P A E) \cdot \text{TruncNorm}(E_{ng} \mu_{ng}^E, \sigma_{ng}^{2E})}$ $E_{ng} = \begin{cases} E_{ng}^* & \text{with probability } acc_{ng}^E \\ E_{ng} & \text{with probability } 1 - acc_{ng}^E \end{cases}$ $\mu_{ng}^E \dots \sim \text{Normal} \left(\mu = \frac{m_{ng}^E / s_{ng}^E + E_{ng} / \sigma_{ng}^{2E}}{1 / s_{ng}^E + 1 / \sigma_{ng}^{2E}}, \sigma^2 = \frac{1}{1 / s_{ng}^E + 1 / \sigma_{ng}^{2E}} \right)$ $\sigma_{ng}^{2E} \dots \sim \text{InverseGamma} \left(a_{ng}^E + \frac{1}{2}, b_{ng}^E + \frac{1}{2} (E_{ng} - \mu_{ng}^E)^2 \right)$
Variances σ^2	$\sigma_g^2 \dots \sim \text{InverseGamma} \left(\alpha_g + K/2, \beta_g + \frac{1}{2} \sum_k (M_{kg} - (PAE)_{kg})^2 \right)$
Signature Inclusion	$p(R = r \dots) \propto \frac{1}{N+1} \left[\prod_{n=1}^N \left(q^{(r)} \right)^{A_n} \left(1 - q^{(r)} \right)^{1 - A_n} \right]^\gamma$
Indicators A	<p>where $q^{(r)} = \begin{cases} 0.4/N & \text{if } r = 0 \\ r/N & \text{if } r \in \{1, \dots, N-1\} \\ 1 - 0.4/N & \text{if } r = N \end{cases}$</p> $A_{nn} \dots \sim \text{Bernoulli} \left(\frac{p_1}{p_1 + p_0} \right)$ <p>where $p_a = \begin{cases} q^a (1 - q)^{1-a} \cdot f(M A_{nn} = a, \dots)^\gamma & \text{in BFI} \\ q^a (1 - q)^{1-a} \cdot [f(M A_{nn} = a, \dots)] \cdot G^{-\frac{1}{2}(K+G)N^{(a)}} & \text{in SBFI} \end{cases}$</p> <p>and $q = q^{(R)}$</p>

 Table A.4: **Gibbs updates** for all models.

B Simulations Appendix

B.1 Detailing runtime of *fast Poisson-Truncated Normal*

We saw in the simulation study with known rank that the fast Poisson-Truncated Normal model is slightly slower than the Normal-Truncated Normal, and Figure B.5 explains why. The added Metropolis steps increase the time required per iteration, but the fast Poisson-Truncated Normal model converges without the need for additional iterations, on average.

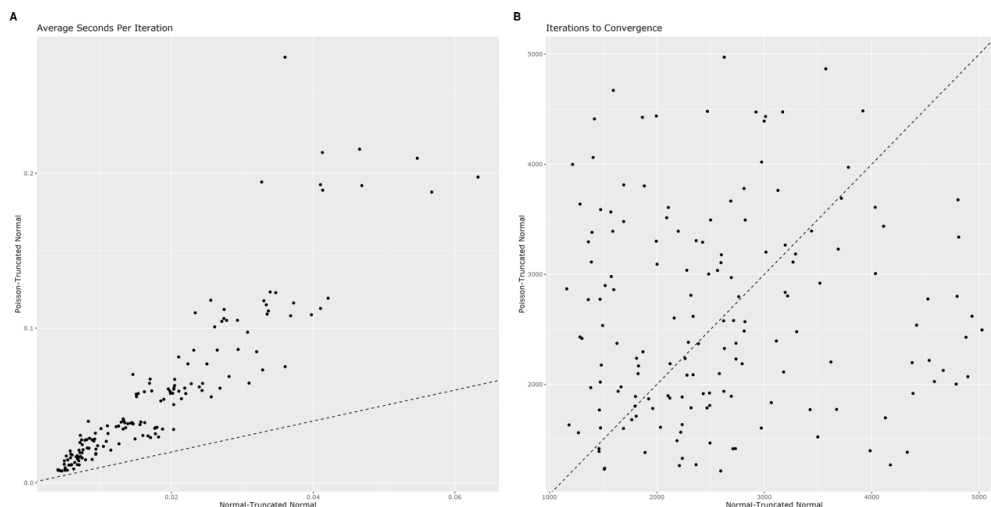


Figure B.5: **Inspecting components of total runtime for Normal-Truncated Normal model (x-axis) vs fast Poisson-Truncated Normal model (y-axis).** Each point is a single simulated dataset from the simulation study with known rank. **a)** comparing average seconds per iteration. **b)** comparing number of iterations to convergence (jitter added for distinct points).

C PCAWG Application Appendix

C.1 Identifying Hypermutated Samples

The total number of mutations per sample, $m_g = \sum_k M_{kg}$, is modeled by a negative binomial mixture model, which is fit using the Expectation-Maximization algorithm [Dempster et al., 1977]. The number of mixture components, $C \in \{1, 2, \dots, 10\}$ is chosen in a two-step fashion: first, if BIC is optimized at 1 component, we say there are no hypermutated samples, and otherwise, we choose the number of components between 2 and 10 to optimize the silhouette score. Samples are assigned to clusters based on the mixture component with the highest a-posteriori probability. Figure C.6 shows the distribution of m_g for each histology group as well as the final clustering into hypermutated and non-hypermutated samples.

C.2 Comparing SBS1 vs SBS6

COSMIC signatures SBS1 and SBS6 are very similar with overlapping spikes in C>T mutations, particularly when followed by G (Figure C.7). SBS1 is a spikier version of SBS6 in that the relative frequency of all C>T mutations *not* followed by G drops to 0.

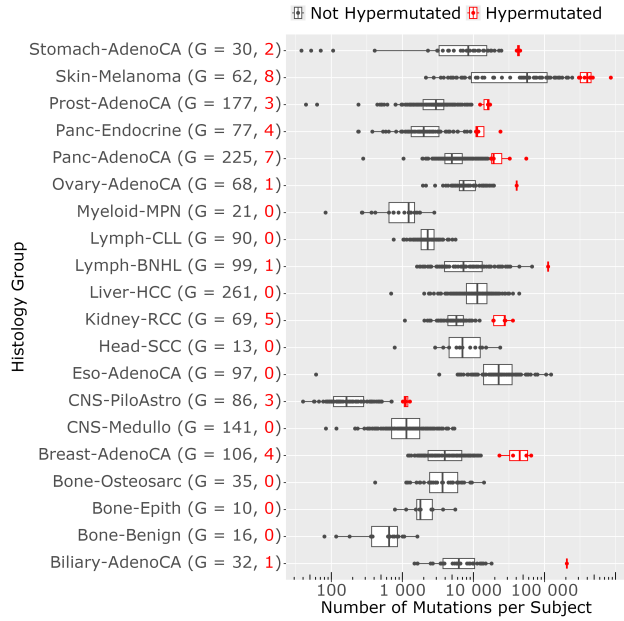


Figure C.6: **PCAWG data: total mutations per sample m_g** plotted for each histology group and colored by hypermutation status. The y-axis labels report the number of cancer genomes G separately for non-hypermutated (black) and hypermutated (red).

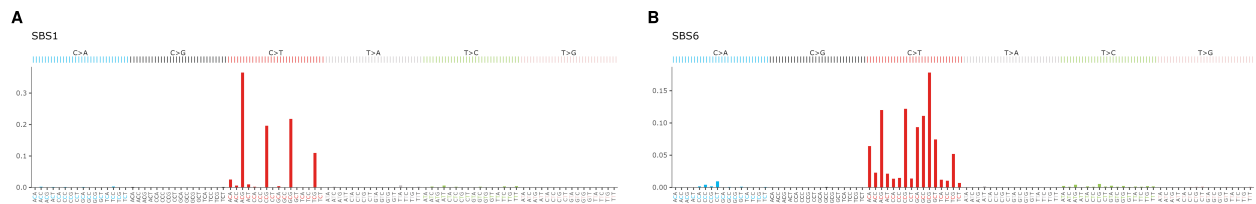


Figure C.7: **COSMIC reference signatures [Consortium, 2020]** a) SBS1. b) SBS6